
Article:
Parry, J.A., Horoshenkov, K.V. orcid.org/0000-0002-6188-0369 and Williams, D.P. (2020) Likelihood maximisation techniques for ranging gunfire over grassland. Applied Acoustics, 164. 107281. ISSN 0003-682X

https://doi.org/10.1016/j.apacoust.2020.107281

Likelihood maximisation techniques for ranging gunfire over grassland

Jordan A Parry[1a], Kirill V Horoshenkov[1a], Duncan P Williams[2]
[1]University of Sheffield, Dept. of Mech Engineering[a], Sheffield, England
JAParry1@Sheffield.ac.uk; K.Horoshenkov@Sheffield.ac.uk;
[2]Defence Science and Technology Laboratory, Salisbury, England
DPWilliams@dstl.gov.uk;

Abstract

A study into acoustic parameter inversion in the presence of a non-moving, homogeneous atmosphere and *grassland* impedance ground is carried out using methods of *likelihood maximisation.* Measured frequency-dependent sound pressure level and power spectra for a blank firing pistol are used to generate simulated data with added Gaussian error to represent variations usually present in real life experiments. Inference is carried out using *maximum likelihood estimation* (MLE) and *maximum a priori* (MAP) where model parameters are either given as known or restricted to some uncertain distribution bounded by realistic conditions. The quality of inference is assessed visually and statistically as the error between the true and inferred predictions for a given propagation range. Application of a prior (MAP) greatly improves inference accuracy compared to the sole maximisation of the likelihood function (MLE). It is shown that the use of a single octave band frequency window does not improve the quality of inference, whereas combinations of several low frequency octave bands do. Exact quantification of the true values of the ground and source height are seemingly less important as range increases beyond $500m$. Although the techniques presented in this paper are for military/security applications, they are readily applicable to other acoustical problems, e.g. source characterisation in engineering noise control. The methods adopted are likely to benefit from higher-dimensional models, i.e. inhomogeneous atmospheres, complex terrain or urban environments.

Keywords

Outdoor sound propagation; Gunfire; Maximum likelihood Estimation; Maximum A Posteriori; Error Analysis;

1 Introduction

Predicting outdoor sound is a complex problem particularly when there is an uncertainty in the parameters involved. This makes the *inverse problem,* or the *inference* of the non-acoustical parameters affecting outdoor sound propagation from the acoustical data a rather difficult task. This is the situation where an array of statistical concepts and methods can be used to infer a parameter while adjusting for the uncertainty present [1]. Only recently has significant works been published by D. K. Wilson et al, removing some of the ambiguity surrounding uncertainty quantification within outdoor sound propagation [2]. Two cases were studied: a simple homogenous atmosphere then a near-ground propagation in a turbulent atmosphere. It showed which sampling methods proved more accurate, dependant on which parameter uncertainty was more dominant. Citing this work, further research by T. Van Renterghem and D. Botteldooren looked at quantifying the variation in downwind sound propagation over a *grassland* impedance ground [3]. A large variation was found, strongly dependent on sound frequency, source height, receiver height, and propagation distance. The variation ranges give insight to this systematic uncertainty when performing short-range measurements. However, the effect of the uncertainties and their interactions is still not well understood.

These works suggest to use statistics in combination with outdoor acoustics to understand the uncertainty the problem presents. The art of using statistically justified methods in the already complex outdoor setting usually requires high-level statistical knowledge combined with thorough understanding of acoustical principles. Otherwise, the inference is likely to yield statistically insignificant results. Extending this work to specific sources can complicate matters further, i.e. gun fire sources which spectrum is limited to very low frequencies of sound. Work on gun detection is of obvious importance in defense applications, yet it is still an understudied area particularly in the case of large-scale outdoor situations. There has been works (e.g. [4]) in which methods for localization of small arms fire using acoustic measurements of muzzle blast with, and without, ballistic shock wave arrivals were studied. It was found that accuracy of detection was greatly dependant on the classification of the firearm and bullet themselves, making wider applicability limited. A more recent paper by one of authors of [4] attempted to expand the model using the *miss angle*, i.e. the angle in which the bullet from a small arms fire passed the acoustic sensor node, to infer the range over a given 2-D space [5]. This method improved by only

having to know a known approximate range for the acoustic impulses i.e. gun barrelling, caliber, rather than requiring exact classification of the firearms and components as in the authors former study. It was shown that the error greatly increased with the increase in miss angle, and it was suggested that the method would be relatively accurate for known stationary geometric areas, i.e. counter-sniper zone. This is an improvement for stationary 3D capture, but there was lot of inherent reliance on known parameters, like impedance ground, and a fair amount of information about the firearm source. More recent work by J. A. Parry et al used a simple *excess attenuation* model, with and without *a priori* knowledge to infer the source range and simulated data for sound propagation from a blank firing pistol [6]. The ground in this instance was assumed to be *vegetative,* creating an *acoustically softer* ground. It was found that errors could be reduced when a priori was applied. A greater accuracy ($\sim \pm 5m$) of range detection was achieved when the likelihood space was filtered in octave bands in the infrasonic frequency range. It was noted that *measuring* the value of excess attenuation directly would require some extra mathematical computation, but this study still showed the powerful accuracy of this method specifically and also how these statistical techniques could be expanded directly to other models.

This paper aims to study the effect of geometrical uncertainties on outdoor sound propagation of a gunshot and performance of some parameter inversion methods. We show that a relatively simple outdoor propagation model and maximum likelihood method can be applied effectively to infer the location of the gunshot with limited prior knowledge at a short and medium range. The study assumes a *grassland* impedance, more similar to wilder areas of United Kingdom. The methods applied also aim to show the effect of specific interactions of uncertainties in the parameters of the model. This paper makes use of two differing statistical ideologies to maximise the *likelihood function*: frequentist and Bayesian. The frequentist method of *maximum likelihood (*or *log-likelihood) estimation* (MLE) makes use of the likelihood function in combination with the mean and variance to gather estimates of given parameters [7]. MLE methods have been successfully used in acoustical research, with good examples in the forward case to evaluate models for impulsive noise propagation [8] or for acoustic source localisation in wireless sensor networks [9]. These works are a good example of how MLE methods can be applied to given uncertain scenarios and used to improve understanding of the effects of a given uncertainty on sound propagation, while also being used for direct parameter inference.

The Bayesian *Maximum a Posteriori (MAP)* method also makes use of the likelihood function, but it also incorporates a *prior,* which is the quantification of beliefs or known knowledge [10]. The use of Bayesian methods is more novel in outdoor sound propagation. A recent study successfully used Bayesian inference to optimise the selection of parameters in models used for sound propagation outdoors [11] and in porous media [12]. They however did not successfully detail the uncertainty itself, perhaps because some departure from model simplicity in their approach [11]. The work by Xiang and Fackler [12] defines the power of Bayesian statistics in application to acoustics in general rather than for outdoor sound propagation. This work demonstrates how Bayesian statistics can be used to improve model selection and parameter inference techniques in acoustics. This work suggests that Bayesian methods have their advantages when applied correctly, but they can easily be misused or overcomplicated meaning that intricacies of the physical effects can be overlooked.

Our paper aims to illustrate how these statistical ideas can be effectively applied to study the uncertainty in outdoor sound propagation and how two different statistical approaches can influence the effectiveness of the inference process and quantified in terms of the inversion error. Simulations are used to mimic the repeated measurement to inform the inference process. It is assumed that sound propagates in a non-moving homogenous atmosphere over a *grassland* impedance ground. The impedance ground, and other source geometry parameters are studied under known and uncertain conditions, solely and in combination, to establish whether or not some particular uncertain conditions have a significant influence on the inference process.

Observed data are synthesised using a popular model for short-/mid-range sound propagation that is assumed to be *perfect*, i.e. given a set of geometrical, ground and source parameters this model would predict the exact true value of the sound pressure at the receiver position. Gaussian (normal) noise is then added to simulate the uncertainties present in the measurements. Observation sample size is kept small ($n = 10$) to test the effects of limiting information on the performance of the model. Estimates of the range are gathered from each sample data set either solely from the *maximisation of the log-likelihood* or via *Maximum a Posteriori* by applying some *prior beliefs* as a statistical function. Estimations are performed for a combination of the parameters being given as known, or uncertain. The uncertainty here is some flat *uniform distribution* where no information on which parameter values are more likely is given. The prior considered here is chosen selectively around the true parameter value with a *normal distribution,* $N(\mu, \sigma^2)$, with a mean (μ) and constant variance (σ^2). Prior beliefs

are only applied to the range parameter. The function will also have its frequency range restricted to specific *octave bands* to further assess whether inference or parameter interactions change compared to the initial broadband frequency range.

The primary question of this paper is: *How well can a simple method recover an unknown range in an outdoor sound propagation setting?* We are also asking: (i) Which, if any, combinations of uncertainty inside parameters cause more errors than others? (ii) What is the effectiveness of simple statistical techniques in inferring the source range? (iii) How effectively the source of a gunshot could be detected, over a grassy floor, using these methods? The answer to the primary question is likely to have an immediate impact on current practices while the other specific questions will help improve the basic understanding of the uncertainty in outdoor sound propagation. This work will also pave the way to further statistical improvements to acoustic inversion methods in the presence of uncertainties, with direct application to improving gunshot detection practices.

This paper is structured in the following manner. Section 2 describes the acoustical model and source characterisation. Section 3 details the statistical likelihood methodologies. Section 4 reviews the results from the simulations, firstly for broadband sounds and then at octave filtered frequency bands. Finally, Section 5 is the conclusions from this study.

2 Research Methods

2.1 Gun source evaluation

Acoustical characterisation of gunfire shows it has three main components: (i) muzzle blast, (ii) mechanical action; and (iii) supersonic projectile [14]. The gun used in this study is a *Bruni Mod. 92 Top Venting 8mm Blank Pistol*. A blank pistol must be used due to the obvious security issues and to obey with the statutory gun law in the UK. This means that the third contributing sound source of the projectile is not present in this experiment. Acoustic recordings of the gunfire are taken in the *anechoic chamber* at the University of Sheffield. The hilt of the gun is placed on the floor and $3m$ away from a GRAS 46AN 1/2" Microphone which is also placed on the floor. The frequency range of this microphone is 0.5 – 10000 Hz. The microphone is connected to a NI DAQ PC and digitised at 1 kHz without any filtering except the anti-aliasing filter provided as standard in the NI DAQ PC. The level of background noise in the chamber was negligibly small in comparison with the level of the gunshot (with the SNR > 100 dB). Recordings made were narrowed down to four *clean* recordings to study the reproducibility of the source spectrum with minimum interference. Figure 1 presents the Fourier spectra plotted against the frequency (ω) in Hertz of the four *clean* (i.e. without unwanted sounds heard during recording) gunshots. The frequency spectra show strong peaks around < 5Hz and 50Hz which level is consistent within $< \pm 1$ dB between individual gunshots. Frequencies over 500 Hz were omitted due to their lack of energy. The time and Fourier spectra look remarkably alike to other experimental data recorded for other types of gunfire [15,16].

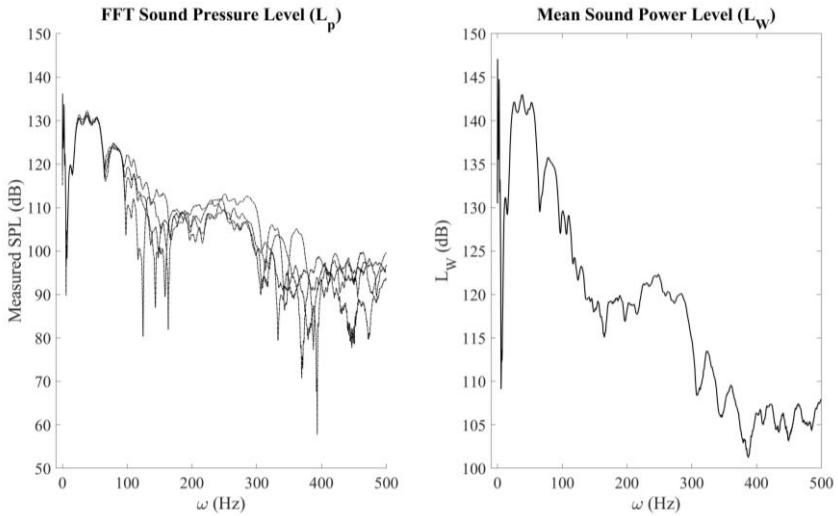

Figure 1: Sound pressure level spectra ($L_{\bar{p}}$) of the gunshot recordings (left) and the mean sound power level (L_W) spectrum (right).

An important quantity that can be established form these recordings is the *sound power level* (SWL or L_w for hereon) of the gunshot. The SWL of the source placed on the ground can be defined as

$$L_w(\omega) = L_{\bar{p}}(\omega) + 10\log(2\pi\bar{r}^2)\ , \tag{1}$$

where $\bar{r}$ is the range from the sound source and $L_{\bar{p}}$ is the *sound pressure level* (SPL from hereon). The range from the source is known to be 3m, resolving the second term in eq. (2.1). The SPL is a measure of the frequency-dependent pressure measured against the reference pressure $\left(p_{ref} = 20 \times 10^{-6}\ \text{Pa}\right)$. The SPL is calculated from

$$L_{\bar{p}}(\omega) = 10\log\left(\frac{p_{av}^2(\omega)}{p_{ref}^2}\right), \tag{2}$$

where $p_{ref} = 20\ \mu Pa$ is the reference sound pressure. The mean is taken from the measured pressures (p_{av}), as seen in the left of Fig.1, to then obtain a given SPL. This gives us a representative frequency dependent SWL of the gunshot (see RHS of Figure 1) ready to be used to generate long range observations.

2.2 Acoustical Predictions

Acoustical predictions are made with one receiver across a 2-D plane as shown in Figure 2. Ignoring problems, such as angle detection for a 3-D sound propagation case allows for better investigation into the underlying uncertainties. In practical applications the measured quantity at the receiver is the SPL. The calculated SWL is used to simulate the SPL $\left(L_p\right)$ that would be measured at a given range. According to the constraints from the assumptions of the homogenous atmosphere and from impedance ground, the frequency dependent SPL at a given range r can be calculated as [17]

$$L_p(\omega) = L_W(\omega) - 10\log(4\pi r^2) + \Delta L(\omega)\,, \tag{3}$$

where ΔL is the *excess attenuation. Atmospheric absorption* is omitted due to its negligible effect at the given lower frequencies. The excess attenuation for a non-moving, homogeneous atmosphere is a measure of the ground effect only and it is calculated as [17]

$$\Delta L = 10\log\left|1 + Q\frac{R_1}{R_2}\exp\left(ik(R_2 - R_1)\right)\right|\ , \tag{4}$$

where k and Q are the wavenumber and spherical wave reflection coefficient, respectively. The distances R_1 and R_2 can be defined as

$$R_1 = \sqrt{r^2 + (z - z_s)^2}\,, \tag{5}$$

$$R_2 = \sqrt{r^2 + (z + z_s)^2}\,, \tag{6}$$

for given source (z_s) and the receiver (z) heights. The spherical wave reflection coefficient (Q) accounts for the effect of the impedance ground on the acoustic pressure amplitude and phase. The equation for the spherical wave reflection coefficient is

$$Q = \left(\frac{Z\cos\theta - 1}{Z\cos\theta + 1}\right) + \left(1 - \left(\frac{Z\cos\theta - 1}{Z\cos\theta + 1}\right)\right)F(w)\,. \tag{7}$$

The angle θ is the incident angle as shown in Figure 2. The function $F(w)$ accounts for the boundary loss factor and it is defined as

$$F(w) = 1 + iw\sqrt{\pi}\exp(-w)\,\text{erfc}(-iw)\,, \tag{8}$$

with $\text{erfc}(-iw)$ being the complimentary error function

$$\text{erfc}(z) = \frac{1}{\sqrt{2\pi}}\int_z^\infty \exp(-t^2)\,dt\,. \tag{9}$$

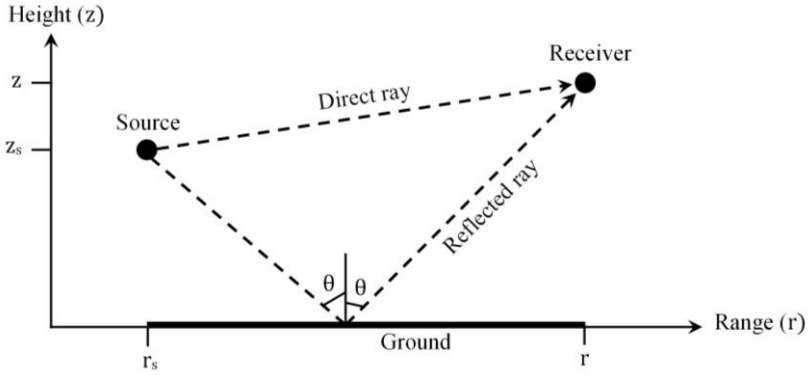

Figure 2: Acoustic scenario in the (r, z) geometry

The parameter Z in eq. (7) is the normalised impedance of the ground, which depends greatly on the ground characteristics. The impedance Z is determined using the model proposed by Horoshenkov et al [18]. This model calculates the acoustic properties of the impedance ground by considering the ground as a porous media with pores of non-uniform cross-section with the median radius $\bar{s}$.

In outdoor sound propagation studies, it is common to refer to the effective flow resistivity of the ground (σ_g). The acoustic impedance model proposed in [18] relates the effective flow resistivity to the median pore size as

$$\sigma_g = \frac{8\eta\alpha_\infty}{\bar{s}^2\phi} e^{6(\sigma_s \log 2)^2}, \tag{10}$$

where η is the dynamic viscosity of air. In the above equation it is common to set the values of porosity (ϕ) and tortuosity (α_∞) to unity and standard deviation in pore size (σ_s) to zero, because for a majority of outdoor ground types their influence on the value of effective flow resistivity is relatively small in comparison with that of the median pore size.

Examples of the excess attenuation spectrum for the given true values, the varying range and grassland impedance, of the input parameters are shown in Figure 3. It is seen how the value of excess attenuation (ΔL) is varies across frequency (ω), exhibiting an oscillatory behaviour with the increase of frequency (ω). The initial geometry effects the interaction pattern, with more *oscillations* occurring as the range is decreased.

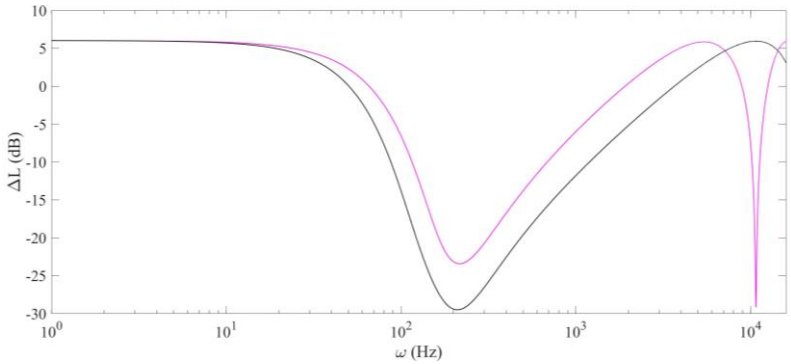

Figure 3: Excess attenuation (ΔL) spectra of due to each combination of parameters and impedance $(\sigma_g = 100\ \text{kPasm}^{-2})$ over a logarithmic scale up to a frequency (ω) of 16 kHz. The ranges given are $250m$ (black line) and $500m$ (magenta line) .

2.3 Generating Observed SPL

Observations are generated by assuming that our acoustical model is *perfect*, or that with given parameters the model would predict the exact observable value i.e. SPL measurement. This assumption allows observations to then be generated by using the predictive model itself with some given *noise*. Initial observations are generated using the SPL model (eq. (3)) with the true heights of the source (h_s) and receiver (h_r) set to 2 m and the

impedance ground has the effective flow resistivity (σ_g) of 100 kPasm^{-2}, which is the typical for *grassland* [19]. The range (r) is assessed at either 250 m or 500 m. The predicted SPL spectrum for the set parameters including the range (r), are shown in Figure 4 as black lines. These predicted SPL show a strong resemblance with the experimental data recorded for similar settings using a 9mm handgun [20], with the differences expected to be due to 1mm decrease in the pistol calibre and lack of projectile in the case of our pistol. The sound propagation model, eq. (3), can be expressed as a function of the input parameters

$$y = f\left(\omega, h_s, r, h_r, \sigma_g, L_W(\omega)\right) . \tag{11}$$

Simulated observations are then repeatedly generated by adding a random, but *controlled,* artificial error to mimic noise within data collection, thus observations,y, are generated via

$$y = f\left(\omega, h_s, r, h_r, \sigma_g, L_W(\omega)\right) + \varepsilon_s . \tag{12}$$

The error applied at every simulation is randomly drawn from the distribution $\varepsilon_s \sim N(0, \sigma_\varepsilon^2)$, with a fixed variance (σ_ε^2) set to 5dB. This error term remains constant across frequency (ω). Normal (Gaussian) error is an acceptable error term to use being supported by the central limit theorem. The added term creates observations that can be $\pm$5dB away from the true value. However, the probability of observing data with such an error decreases the further it moves from the true value. This error value is approximately equal to 10% of the difference between the highest and lowest observable SPL. The range for which the generated observations can be measured are seen via the dashed limits in the plots of the true SPL (dashed lines in Figure 4).

For our investigations a small amount of observations $(n = 10)$ are used to test how effective the parameter estimation can be using each statistical technique and little information present in the model. It is known that smaller sample sizes increase the uncertainty present in the estimation techniques. This is a key part in the investigation to compare how applicable this methodology is in practice in the presence of such systematic uncertainty.

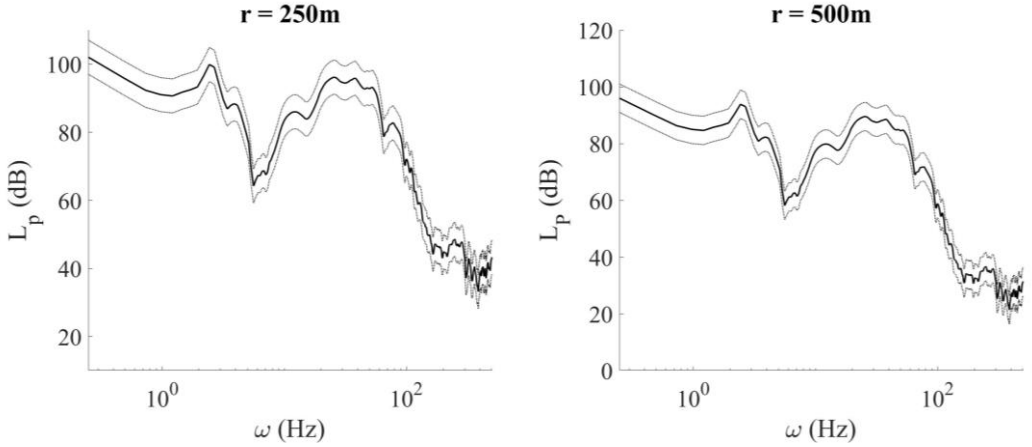

Figure 4: Predicted SPL (L_p) against frequency (ω) for the different ranges (r) over a logarithmic scale (solid line). Error margins for observation generation are superimposed (dashed lines).

In practice it is common to analyse the sound pressure level in octave bands. This analysis will become useful as shown in the following sections. The octave bands used in our analysis are defined in Table 1 in accordance with the ISO 266 [21]. Each band is denoted as B with a relevant subscript. This is merely to improve ease during visual analysis and scission.

Octave 1/1 Band (B_n)	Lower Limit (Hz)	Centre Frequency (Hz)	Upper Limit (Hz)
B_0 (Band 0)	0.24	1	1.41
B_1 (Band 3)	1.41	2	2.82
B_2 (Band 6)	2.82	4	5.62
B_3 (Band 9)	5.62	8	11.2

B_4 (Band 12)	11.2	16	22.4
B_5 (Band 15)	22.4	31	44.7
B_6 (Band 18)	44.7	63	89.1
B_7 (Band 21)	89.1	125	177
B_8 (Band 23)	177	250	355
B_9 (Band 25)	355	500	710

Table 1: Octave bands, in keeping with ISO 266.

3 Statistical techniques

3.1 Maximum Log-likelihood Estimation (MLE)

The first statistical method uses the frequentist ideology of maximising the *likelihood function* at a given parameter. For this, we assume that the observations are distributed *normally*. This allows us to describe the observations with a normal probability density function (PDF for hereon), the familiar bell-shaped curve, defined as

$$f_N\left(x_j|\mu_o,\sigma_o^2\right) = (2\pi\sigma_o^2)^{-\frac{1}{2}}\exp\left(-\frac{1}{2\sigma^2}\left(x_j-\mu_o\right)^2\right). \tag{13}$$

The mean (μ_o) and variance (σ_o^2) in this case are the true and known values that describe how the observations, e.g. sound pressure or sound pressure level, are distributed. The set of parameters then define a normal distribution, $\theta = (\mu, \sigma)$, are the values that objective variables the likelihood function attempts to maximise simultaneously. The remaining information required by the likelihood function is the *observables,* i.e. recorded data. Each new observable brings information into the function, allowing for the likelihood to define a better set of θ that describes the likelihood's of new data [7]. If we define our sample group of observations as $\boldsymbol{x} = \left(x_1, \dots, x_j\right)$ the likelihood function can be written as

$$\mathcal{L}(\theta|\boldsymbol{x}) = \prod_{j=1}^{n} f_N\left(x_j|\mu,\sigma^2\right), \tag{14}$$

where n is the total number of observables (x). The function in eq. (14) can be further simplified with some manipulation to

$$\mathcal{L}(\theta|\boldsymbol{x}) = \prod_{j}^{n}(2\pi\sigma^2)^{\frac{1}{2}}\exp\left(-\frac{1}{2}\frac{\left(x_j-\mu\right)^2}{\sigma^2}\right). \tag{15}$$

$$\mathcal{L}(\theta|\boldsymbol{x}) = (2\pi\sigma^2)^{-\frac{n}{2}}\exp\left(-\frac{1}{2\sigma^2}\sum_{j}^{n}\left(x_j-\mu\right)^2\right). \tag{16}$$

Taking the log transform $\log\left(\mathcal{L}(\theta|\boldsymbol{x})\right) \to \ell(\theta|\boldsymbol{x})$, gives the *log-likelihood function,* a better-defined function which is also algebraically easier to compute. The log-likelihood $\ell(\theta|\boldsymbol{x})$ can be rewritten as

$$\log\left(\mathcal{L}(\theta|\boldsymbol{x})\right) = \ell(\theta|\boldsymbol{x}) = -\frac{n}{2}\log(2\pi)\ \dots$$
$$\dots -\frac{n}{2}\log(\sigma^2) - \frac{1}{2\sigma^2}\sum_{j}^{n}\left(x_j-\mu\right)^2. \tag{17}$$

It is important to note at his stage the key relationship, and differences between likelihood and probability. The following relationship is known to be true

$$P(\boldsymbol{x}|\theta) \equiv \mathcal{L}(\theta|\boldsymbol{x}). \tag{18}$$

While colloquial in use, the terminology is equally misused as the same thing in daily life whereas each function is doing something different. For any given distribution, $P(\boldsymbol{x}|\theta)$ defines the *probability* for observing data $\boldsymbol{x}$, for

given set of parameters θ. Meanwhile, $\mathcal{L}(\theta|\boldsymbol{x})$ describes the how *likely* taking the set of parameters inside θ is for given values of the observables $\boldsymbol{x}$**.** The important difference is that each function is asking question about the data or parameters values. Manipulation of these statistical ideas is what allows us to perform inferences on our observables and thus study the effects of error and uncertainty on our given, or in a matter of fact any, acoustical scenario.

Our study manipulates the θ set in combination with the model that generates $\boldsymbol{x}$, to infer parameters from inside the later model. The variance (σ^2) is given as known being assumed equal to the initial variance inside our observations. Thus, the variance of $\ell(\theta|\boldsymbol{x})$ is equal to σ_ε^2 which was set to 5 dB in eq. (12). The mean (μ) is also given as known, but uses the given acoustical model in *perfect* conditions. The mean (μ) is calculated using the same method that generates our sample data, requiring the situation-dependant true values of frequency (ω), source geometry (h_s, r) and effective flow resistivity of the ground (σ_g), but no noise added. This can be used as it is still assumed that, given a set of parameters, the model would predict the *perfect* result which would also be equivalent to the mean of a data set containing noise. The inference process then relies on the values inside our predictive model (eq. (3)) would maximise the likelihood to these given set of θ, i.e. which set of parameter values would be most likely.

It is well understood that Bayesian methods become equivalent to frequentist methods as the number of observations becomes *large.* Limiting the initial information available to the likelihood function allows for investigation into the performance of the MLE (and soon to be discussed MAP) method. The increase in observation size, albeit small, will assess if any improvements can be detected with such a smaller addition of initial information.

The $\omega - r$ space is generated by using given values of each parameter. Frequency points (ω) cover the frequency range for sound generated by the gunshot (see Section 2.2), usually $1 \leq \omega \leq 500\text{Hz}$. The r space covers the range of $100\text{m} \leq r \leq 650\text{m}$. The definition of the r space should not be confused with the application of a *prior* previously discussed in Section 3.2. Other parameters, specifically the source height (h_s) and effective flow resistivity of the ground (σ_g), are allowed to be distributed, i.e. incorporate uncertainty, for further study into their interactions. In the most uncertain case, with both parameters unknown, draws are taken from a *uniform distribution* for each parameter for every individual simulation run. A *uniform distribution,* $\text{U}\sim[a, b]$, creates a distribution between a lower bound (a) and upper bound (b) with an equally weighted probability of drawing any number between these limits. This allows for the physical constraints of reality to be applied without any *a priori* knowledge, while simulating complete uncertainty around the parameter. The distributions drawn from are

$$\tilde{h}_s \sim U[0.1,10]\,, \tag{19}$$

$$\tilde{\sigma}_g \sim U[20000,200000]\,. \tag{20}$$

The distribution of the height (eq. (19)) has its upper bound at 10m as higher source heights are also known to be subjected to atmospheric influences [17] which the model adopted here does not account for. The distribution of the flow resistivity of the impedance ground (eq. (20)) is chosen to encompass variations in the experimental data recorded for this type of grassland [19] we are assuming to be present.

The values of the $\omega - r$ space that best maximise the given combination of likelihood parameters (θ) can now be located. According to the most uncertain case, eq. (17) can be rewritten as

$$\ell\left(\theta|\boldsymbol{y}, \omega, h_s, r, \sigma_g\right) = -\frac{n}{2}\log(2\pi) - \frac{n}{2}\log(\sigma_\varepsilon^2) \;\ldots$$
$$\ldots - \frac{1}{2\sigma_\varepsilon^2}\sum_{a=1}^{n_\omega}\sum_{b=1}^{n_r}\sum_{j=1}^{n}\left(y_j - f\left(\omega_a, \tilde{h}_s, r_b, \tilde{\sigma}_g\right)\right)^2\,. \tag{21}$$

In the case when the source height (h_s) and/or impedance (σ_g) are known they simply have the distributions $(\tilde{h}_s, \tilde{\sigma}_g)$ replaced with the respective true, and unchanging, values $(2\text{m}, 100\text{kPasm}^{-2})$. This likelihood function uses n observations to generate a $n_\omega \times n_r$ space over n_ω and n_r points for frequency (ω) and range (r), respectively. In simple terms, the maximised value is located in the space related to the *best estimate* of r, at a specific frequency for given or unknown source height and impedance.

3.2 Semi-Bayesian Maximum a Posteriori (MAP)

The second method requires the understanding of *Bayes' theorem*. Bayes' theorem is defined as [10]

$$P(\theta|\boldsymbol{x}) = \frac{\mathcal{L}(\theta|\boldsymbol{x}) \times P(\theta)}{P(\boldsymbol{x})}\,, \tag{22}$$

where $P(\theta|\boldsymbol{x})$ is the *posterior*, $P(\boldsymbol{x})$ is the *evidence,* $P(\theta)$ is the *prior* and $\mathcal{L}(\theta|\boldsymbol{x})$ is the likelihood function. The likelihood function is defined the same way as in Section 3.1, while the prior is the PDF of beliefs about θ. The application of a prior is used to import knowledge, or the absence, into the given statistical procedure. The posterior is the PDF that uses these beliefs in combination with the likelihood to generate a probability function of θ for a given set of data. The evidence term normalises the function to a true PDF, however is generally difficult and expensive (computational) to compute. The MAP procedure avoids this by disregarding this term. The only value of interest to us in the posterior is the *best estimate* which happens to be the easily-obtainable peak of the distribution, which is *proportional* to the combination of the prior and likelihood. This method reduces eq. (22) to

$$P(\theta|\boldsymbol{x}) \propto \mathcal{L}(\theta|\boldsymbol{x}) \times P(\theta)\,. \tag{23}$$

Removal of the evidence term greatly reduces computational time, without removing the ability to gather a best estimate of a parameter. Similar to the MLE method, the reduced Bayes equation (eq. (23)) can be log-transformed to

$$\log\big(P(\theta|\boldsymbol{x})\big) \propto \ell(\theta|\boldsymbol{x}) + \log P(\theta)\ . \tag{24}$$

The log-transformed prior can be better interpreted here as a penalty term. The log of a probability is always negative, increasing in magnitude for a decreasingly small probability. The application of log here reduces the likelihood function at positions where the prior is less-confident. It also reduces the likelihood to $-\infty$ in areas outside of the coverage of the prior, due to the log of zero [10].

The prior applied in this instance is a normal, centred around the mean $(\mu_0 = 250m, 500m)$ with a standard deviation of $15m$, thus the distribution covers approximately $\pm 50m$ either side of the given mean. A completely flat prior could have been used in principle, especially in situations where reality constraints motivate it i.e. a uniform distribution that installs cut-offs at values that are known physical impossibilities. However, a flat normal is already applied, thus uniform priors are deemed unnecessary to the narrative of this paper.

3.3 Performance Metrics

To investigate the effectiveness of the inference process and the effects of uncertainties in parameters, we study the *errors* in relation to the predicted values and the true value. We make use of MATLAB™ (and the ShARC supercomputer facilities at the University of Sheffield) to repeatedly simulate a small set of observations ($n = 10$), maximise the likelihood over the $\omega - r$ parameter space for given parameter values, either known or randomly drawn from given distributions, then find the *best-estimate* before and after a prior is applied. The ω space is also analysed in the octave band bounds defined in Table 1.

The error (ε_r) is then found as the difference between a simulation's estimate of the range and the true value of range

$$(\varepsilon_r)_i = (r)_i - r^* \quad \text{for} \quad i \in [11000]. \tag{25}$$

The error is investigated in both *relative* and *absolute* terms. The relative error will allow insight into the *direction* of the incorrect estimations (i.e. whether an under or over estimation was made) while the absolute error is independent of direction.

A substantial number of errors $(n_\varepsilon = 1000)$ are generated to allow the error set to be explored visually and numerically and to minimise the error from the sampling process. Additionally, two more statistics can be investigated: (i) mean absolute error (MAE); and (ii) root mean squared error (RMSE). Both use the previously defined ε_r to analyse the inference process across the entire set of errors. The MAE is the arithmetic mean of the modulus of the errors (eq. (26)), while the RMSE is the root of the arithmetic mean of the square of the errors (eq. (27))

$$\mathrm{MAE} = \frac{1}{n_\varepsilon}\sum_{i=1}^{n_\varepsilon}|(\varepsilon_r)_i| \ , \tag{26}$$

$$\mathrm{RMSE} = \sqrt{\frac{1}{n_\varepsilon}\sum_{i=1}^{n_\varepsilon}((\varepsilon_r)_i)^2} \ . \tag{27}$$

The MAE allows for an insight into the overall average error, while the RMSE is another way of calculating the average error, but it is far more punishing to larger errors, i.e. more *weight* is given to larger errors. Both errors are *independent* of direction, i.e. whether the average estimate overestimates or underestimates the given true value. Visual analysis will be used to assess the under and/or overestimations that may occur

4 Results

4.1 Inference Using Broadband Data

The results of the analysis of errors using broadband sound pressure level data is presented in Table 2. This table shows the MAE, RMSE and absolute maximum error for the simulations for the combinations of known or unknown parameter. These data were drawn from the respective error distribution. The results from each statistical method are also compared.

r^* (m)	h_s (m)	σ_g (kPasm^{-2})	Method	MAE (m)	RMSE (m)	Abs. Max. (m)
250	2	100	MLE	124.74	127.26	150
			MAP	23.53	30.1634	96.05
		$\tilde{\sigma}_g$	MLE	122.55	125.64	150
			MAP	23.53	30.16	96.05
	$\tilde{h}_s$	100	MLE	123.24	126.48	150
			MAP	23.58	30.21	96.05
		$\tilde{\sigma}_g$	MLE	120.89	124.71	150
			MAP	37.85	48.25	202.9
500	2	100	MLE	294.43	300.21	500
			MAP	44.63	57.81	211.71
		$\tilde{\sigma}_g$	MLE	295.1	301.21	399.45
			MAP	44.67	57.83	211.72
	$\tilde{h}_s$	100	MLE	295.9	302.47	400
			MAP	44.72	57.87	211.72
		$\tilde{\sigma}_g$	MLE	300.29	306.63	400
			MAP	44.77	57.91	211.71

Table 2: Collated statistics of error (ε_r) from each simulation. Each row follows the selection of initial parameters, known or drawn from a given distribution, then for the given statistical method used.

Overall errors estimated while using MLE alone are relatively large, being on average 50% and 60% of the true range when the true range (r^*) is 250m and 500m, respectively. Application of a priori, using the MAP method, greatly reduced errors to within 10% of the true range.

The differences in the MAE and RMSE are negligibly small ($< 0.05\ m$) between most simulations where the true range (r^*) is 250m. In addition, the difference between error statistics when the true range is 500 m are also negligibly small ($< 0.1\ m$) when using the MAP method in all conditions. However, when the true range is 250m, and both the flow resistivity of the ground (σ_g) and source height (h_s) where initially unknown, a large jump in error can be seen when the MAP method is used. The MAE increased by ~15m, the RMSE by ~20m and the absolute maximum error increased by ~100m. It is likely that the increase in extreme outliers has dragged the average errors particularly in the case when both the source height (h_s) and flow resistivity of the ground (σ_g) have varied due to the uncertainty present. This effect is not seen when the true range (r^*) is increased to 500m, which indicates the interaction effects of these uncertainties may either be increased by reducing range, or the opposite, the interfering effects of the uncertainties being reduced as the true range (r^*) is increased.

The negligible differences between the statistics of error when uncertainties are imported to various parameters, may be influenced by a relatively small sample of observed data ($n = 10$) in the model. Studying interactions with various levels of initial data in the model is outside the scope of this paper, and it would require repetition of the methods used here with such variations present. They also would inherently be affected by the distribution choice, specifically the effective flow resistivity of the ground (σ_g) being a distribution that covers various recorded values for *grassland.* More acoustically harder grounds *urbanised areas, water,* can have different effects.

4.2 Visualisation of Errors

Visualisation of errors (ε_r) is done using three different plots: (i) a PDF of estimates; (ii) a PDF of the absolute errors; and (iii) the *cumulative distribution function (CDF* from hereon) of the absolute errors. The first allows for insight into the general distribution of where estimates were made in relation to the true value and differences in over and underestimations. The second plot of absolute error defines the probability of the error, no matter whether it is over or under. The CDF of absolute error can be used to visualise the cumulative probability of the defined error. Kernel density estimation (`ksdist` function in MATLAB™) is used to produce smoothed curves that are visually easier to assess. This is deemed acceptable due to the large sample size in each case $(n_\varepsilon = 1000)$.

Visualisations are presented in Figure 5 $(r^* = 250m)$ and Figure 6 $(r^* = 500m)$. Each subplot of a given PDF/CDF contains multiple lines, each representing the results for simulations with the varying input uncertainty, i.e. either only r is unknown, or r and σ_g are unknown or r, σ_g and h_s are unknown. The results presented in Figure 5 suggest that in the short-range case $(r^* = 250m)$ the ineffectiveness of the sole maximisation of the likelihood (MLE) is obvious (as also seen in Table 2). Estimates are centred around the minimum possible value of r set in the model, with a positive skew allowing for a smaller proportion of better estimates, as well as over-estimations (top-left in Figure 5). The PDF of absolute error (top and mid rows in Figure 5) shows that the majority of errors are greater than 100m, which is confirmed by the CDF of absolute error (top-right in Figure 5) where there is a 20% chance of getting an error of less than $\sim 100m$ and 80% chance of getting an error of smaller than $\sim 140m$. The differences between the simulations when all to none of the initial parameters are known are not clear for the MLE method for the true range (r^*) of 250m (top row in Figure 5). However, there is some indication that allowing the effective flow resistivity of the ground (σ_g) to vary may decrease the error slightly, but the magnitude in which the peak (and distributions generally) is flattened here is too small to state as fact.

The application of a prior (MAP method) greatly improves estimations (bottom row of Figure 5). The spread of estimates (bottom-left of Figure 5) is more symmetric around the true range $(r^* = 250m)$, with a negative skew away from this value. When the source height (h_s) and effective impedance of the ground (σ_g) are unknown, the distribution of estimates is far flatter, yet more symmetric around the true value, showing tails containing more overestimations than the related simulations while using the MLE. This confirms the findings (see Table 2) that the error is increased in the most uncertain simulation due to the allowance of larger overestimations rather than underestimations. The MAP method leads to the PDF of absolute error (bottom and mid row in Figure 5) becoming flipped, peaking around zero error with tail decreasing toward larger errors. The most uncertain case is less strongly peaked leading to an increase in size and frequency of large errors. All other simulations seem to be highly probable to be less than $\sim 30m$, with a large drop to a *step* appearing to around $\sim 50m$. The likelihood of an error larger than 50m lower substantial, before tailing out to the maximum error. The CDF (bottom-right of Figure 5) shows the reduction in error compared to the MLE, with a 20% chance of error of less than $\sim 5m$ and 80% chance of an error less than $\sim 40m$. These probabilities are weakened by the case where initial parameters are unknown, with only an 80% chance of less than $\sim 55m$, yet this is substantially better than the MLE case with the least uncertainty. Practical application shows how effective a single simulation could be for inference, giving a user with data ready a value within seconds, with great confidence while using the MAP method. More simulations would be needed for confident predictions with the MLE

All MAP simulations (see bottom row in Figure 5) show far less difference between each distribution, with each plot being smoother and almost exactly alike when compared to the MLE results (see top row in Figure 5) where each plot *oscillates* over one other i.e. each distribution is higher and lower than the others at multiple points. This indicates that the MAP method may itself smooth out small artefacts from varying the uncertainty in other parameters in the model that are not the direct object of the inference. The MAP method does highlight a reduction in likleihood in the most uncertain case (see blue plot at the bottom row in Figure 5), which is not seen in any

other simulations. It is not clear what causes this simulation to be so different, but it seems that the increase in degree of uncertainty is the most likely reason for this difference.

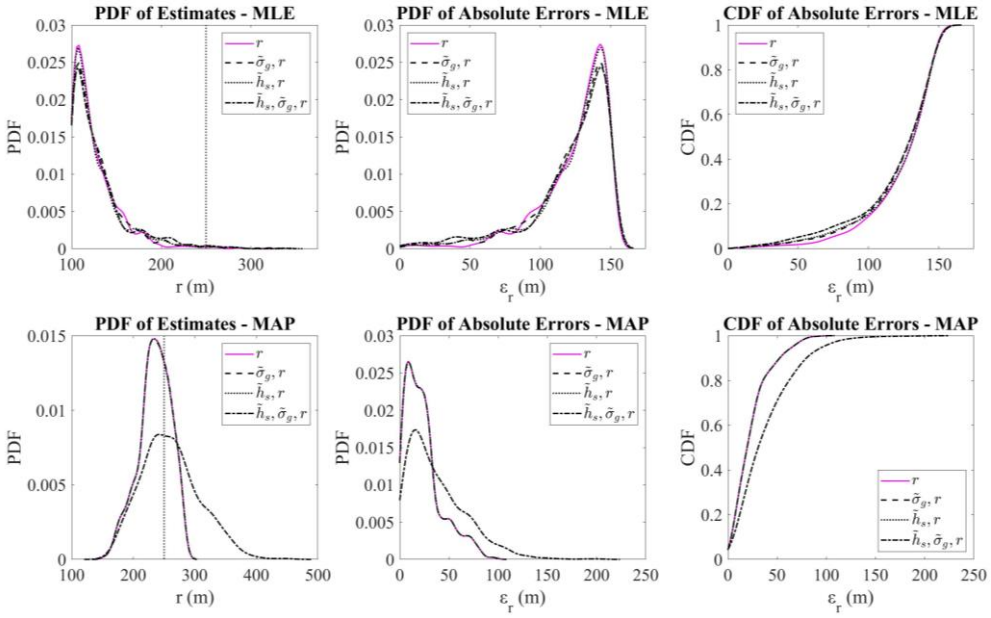

Figure 5 : Kernel distributions for the PDF of estimates (first column), PDF of absolute errors (second column) and CDF of absolute errors (last column) for each simulation of varying uncertainty at $r^* = 250m$. Top and bottoms rows show the results from using the MLE and MAP methods, respectively. The true range value is superimposed (dashed line) in the PDF plot of estimates. Each line represents which initial parameters were uncertain as defined in each legend.

Increasing the true range to $r^* = 500m$ leads to the results shown in Figure 6. The performance of the MLE method is similar to that observed in the case of $r^* = 250m$ (see top-left graph in Figure 5) with a similar distribution of the range and error estimates (see top-left graph in Figure 6). There is a strong peak at the lowest range that the model accepts, with a decreasing probability as the estimate value increases. The distribution of absolute error (top-mid rows in Figure 6) shows a strong peak around 300m tailing off with some negative skew towards small errors. The CDF of absolute error (see top-right in Figure 6) shows that an increase in range reduces performance, where now there is only a 20% chance of the range being less than ~250m out and 80% chance of being greater than ~250m. Differences between simulations in the three plots (see top row in Figure 6) are due to the fact that the uncertainties present are less erratic (or less oscillatory). The peak in each of distribution becomes increasingly flatter as more uncertainty is present (from initial parameters).

The MAP method at this range improves the estimation and reduces the discrepancies between the differing levels of uncertainties from initial parameter selection. The distribution of estimates (see bottom-right graph in Figure 6) shows a distribution around the true value (r^*) close to normal with a negative skew. There is evidence of another peak in the distribution around 450m range. The distribution of the absolute error (see bottom-middle graph in Figure 6) is strongly centred around 5m, with the second peak around 50m. There is a long tail in the distribution showing that larger errors (100m+) are highly unlikely in this case. The CDF (bottom-right graph in Figure 6) shows the effectiveness of the MAP method for errors with a 20% chance of being within 5m and an 80% chance of being within 50m. All of the simulations, of any given initial uncertainty, are near-identical (see bottom row in Figure 6). Even the most uncertain case (source height (h_s) and impedance ground (σ_g) being uncertain) is now no longer a visible different distribution, unlike when the true range was less $(r^* = 250m)$ (bottom row in Figure 5). A recent study by the authors highlighted how the impedance in particular uncertain geometries and statistical behaviour can affect inferences using certain methods [22]. This is likely why the simulations with multiple uncertainties are more strongly affected in the MAP methods at the shorter range $(r^* = 250m)$, yet the increase in range reduces this effect.

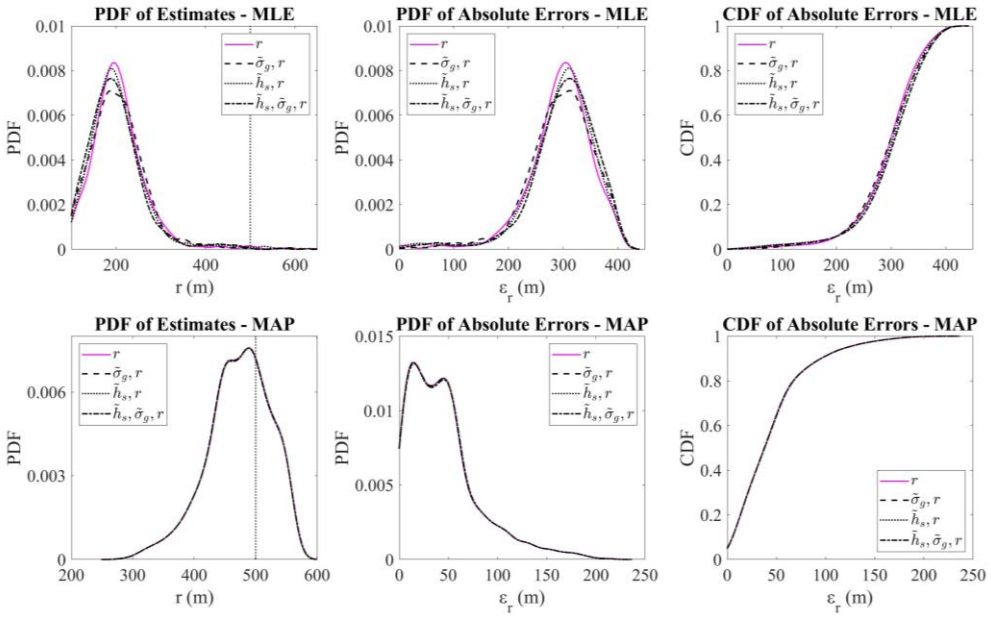

Figure 6 : Kernel distributions for the PDF of estimates (first column), PDF of absolute errors (second column) and CDF of absolute errors (last column) for each simulation of varying uncertainty at $r^* = 500m$. Top and bottoms rows show results from using the MLE and MAP methods, respectively. The true range value is superimposed (dashed line) in the PDF plot of estimates. Each line represents which initial parameters were uncertain as defined in each legend.

4.3 Interactions of Uncertainties

Since draws were taken from distributions for the unknown parameters, source height (h_s) and/or effective flow resistivity of the ground (σ_g), they can be compared to the final estimate determined via the inference. This will enable us to study the sensitivity of such parameter/s while using MLE/MAP methods with the given conditions, i.e. differing range, low initial data source, *grassland* impedance ground against the final inferred range. Scatter plots are used to compare when either the flow resistivity of the ground (σ_g) or source height (h_s) are uncertain to their relevant error from the inference (see Figures 7 and 8). The dots shown in Figures 7 and 8 correspond to the realisations simulated with the proposed statistical methods. When both the effective flow resistivity of the ground (σ_g) and source height (h_s) are uncertain, a grayscale surface plot is used (see Figure 9) to show maps for the error as a function of the range and flow resistivity. These graphs highlight behaviour patterns in the uncertainty that are affecting such inference processes.

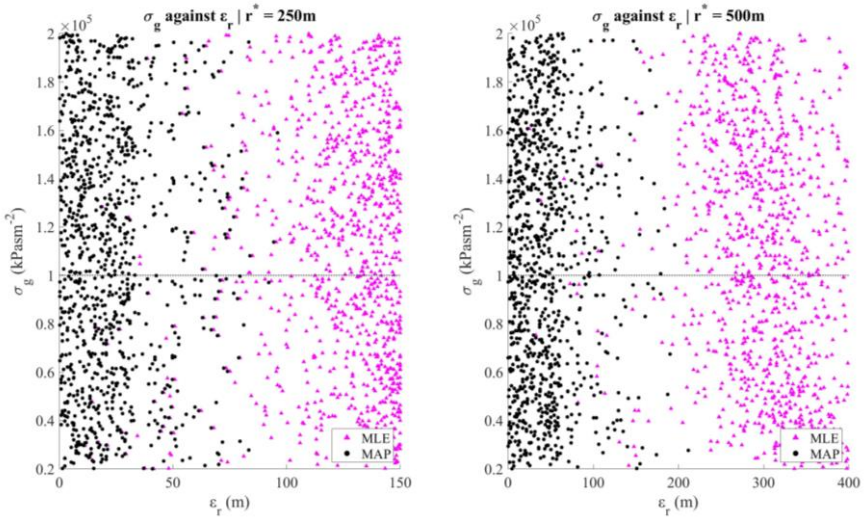

Figure 7: Draws from $\tilde{\sigma}_g$ against their related ε_r for both statistical methods for $r^* = 250m$ (left) and $r^* = 500m$ (right). The true value of the effective flow resistivity $\left(\sigma_g = 100\text{kPasm}^{-2}\right)$ is superimposed (dashed line).

The first parameter investigated is the effective flow resistivity of the ground $\left(\sigma_g\right)$ taken across all possible values $\left(\tilde{\sigma}_g\right)$ against its related absolute error (ε_r). This is achieved by taking the absolute difference from the inferred value and true value while using a drawn value of σ_g (see Figure 7). The MAP method is shown to be far more effective than the MLE method in terms of the value of error. This is true for the both true ranges (r^*) studied in this work. The results presented in Figures 7 and 8 show that the error is not sensitive to the initial draw of σ_g. Although, the MLE results for a true range $r^* = 500$m tend to have smaller errors when a higher value of the effective flow resistivity $\left(\sigma_g\right)$ is drawn (see right plot in Figure 7). It is not thoroughly clear why this would be the case.

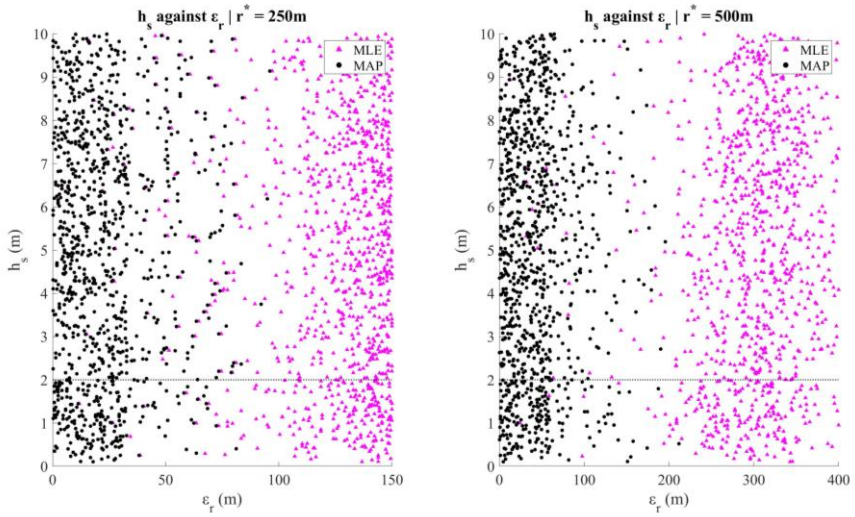

Figure 8: Draws from $\tilde{h}_s$ against their related ε_r for both statistical methods for $r^* = 250m$ (left) and $r^* = 500m$ (right). The true value of the source height $(h_s = 2m)$ is superimposed (dashed line).

Plotting the draws from the source height (h_s) instead of the flow resistivity of the ground $\left(\sigma_g\right)$ shows similar behaviour (see Figure 8). The MAP method again has greater accuracy than the MLE, with no obvious sensitivity to the draw of the source height (h_s) at initialisation. There is some indication that at the range of 500m the MLE method performs slightly worse as the drawn value of source height (h_s) increases. It is known that the increased height would greatly affect the ground interference patterns, yet an overestimation of 8m (as 10m is the maximum overestimated source height allowed) does not seem to prevent the model from inferring the true range (and close to it).

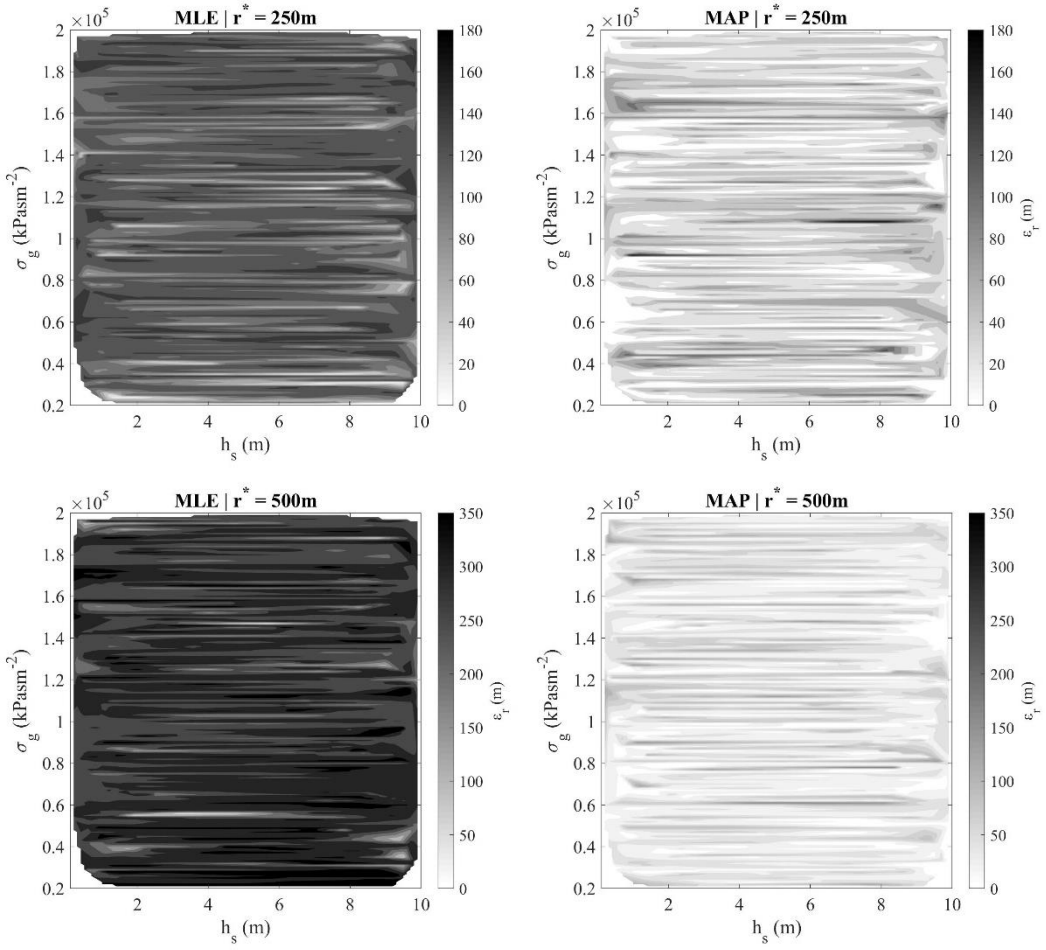

Figure 9: The absolute error plotted as a function against the draws of source height (h_s) and effective flow resistivity of the ground (σ_g) for the two ranges. Error is depicted using a colour gradient. Top and bottom rows show r^* as 250m and 500m, with left and right columns the MLE method and MAP method respectively.

The interactions between the draws and the given error (ε_r) are harder to visualise. Figure 9 plots the error against the source height and effective flow resistivity of the ground. The absolute error is depicted using a colour map with white being no error and black being the maximum error of 180m and 350m for the true range of 250m and 500m, respectively. Horizontal bands can be seen in the surface plots in Figure 9. This means that small variations in the source height (h_s) for a given effective flow resistivity of the ground (σ_g) do not strongly affect the quality of inference, whereas small variations in the effective flow resistivity of the ground (σ_g) for a selected source height (h_s) do. This hints that quantification of the ground impedance may be more important than the source height in situations where both are unknown quantities. These findings are supported by the fact that the so-called "ground effect" is more important for low-height sources than sources at higher altitude, a well-known fact in acoustics, with greatly developed definitions and reasoning explained in well by Solomons [17].

4.3 Inference Using Octave Band Data

Additionally, inference is studied in octave frequency bands and compared against that obtained for the broad band spectrum. This enables us to assess the effect that specific frequency restrictions would have on the inference quality. Table 3 presents the error statistics for each combination of known or unknown (and therefore drawn from the respective distribution) parameters. Only the best and worst performing bands (using bandwidths defined in Table 1) are shown. Best and worst are taken to be the smallest and largest values of error respectively. Unlisted bands are only assessed visually later.

r^* (m)	h_s (m)	σ_g (kPasm^{-2})	Method	MAE (m)		RMSE (m)	
				Best	Worst	Best	Worst
250	2	100	MLE	B_0: 55.3	$B_{3,7,8,9}$: 150	B_0: 70.96	$B_{3,7,8,9}$: 150
			MAP	B_0: 34.16	$B_{3,7,8,9}$: 150	B_0: 41.66	$B_{3,7,8,9}$: 150
		$\tilde{\sigma}_g$	MLE	B_0: 55.04	$B_{3,7,8,9}$: 150	B_0: 70.82	$B_{3,7,8,9}$: 150
			MAP	B_0: 55.04	$B_{3,7,8,9}$: 150	B_0: 41.67	$B_{3,7,8,9}$: 150
	$\tilde{h}_s$	100	MLE	B_0: 56.42	$B_{3,7,8,9}$: 150	B_0: 72.18	$B_{3,7,8,9}$: 150
			MAP	B_0: 56.42	$B_{3,7,8,9}$: 150	B_0: 41.67	$B_{3,7,8,9}$: 150
		$\tilde{\sigma}_g$	MLE	B_0: 56.73	$B_{3,7,8,9}$: 150	B_0: 72.55	$B_{3,7,8,9}$: 150
			MAP	B_0: 56.73	$B_{3,7,8,9}$: 150	B_0: 48.24	$B_{3,7,8,9}$: 150
500	2	100	MLE	B_0: 190.21	$B_{7,8,9}$: 400	B_0: 233.66	$B_{7,8,9}$: 400
			MAP	B_0: 62.63	$B_{8,9}$: 400	B_0: 76.7	$B_{8,9}$: 400
		$\tilde{\sigma}_g$	MLE	B_0: 188.27	$B_{8,9}$: 400	B_0: 231.83	$B_{8,9}$: 400
			MAP	B_0: 62.63	$B_{8,9}$: 400	B_0: 76.7	$B_{8,9}$: 400
	$\tilde{h}_s$	100	MLE	B_0: 187.06	$B_{8,9}$: 400	B_0: 230.16	$B_{8,9}$: 400
			MAP	B_0: 62.63	$B_{8,9}$: 400	B_0: 76.7	$B_{8,9}$: 400
		$\tilde{\sigma}_g$	MLE	B_0: 189.02	$B_{8,9}$: 400	B_0: 232.57	$B_{8,9}$: 400
			MAP	B_0: 62.64	$B_{8,9}$: 400	B_0: 76.7	$B_{8,9}$: 400

Table 3: Collated statistics of error (ε_r) from each simulation, portraying the best and worst performing octave bands. Each row follows the selection of initial parameters, known or drawn from a given distribution and for the given statistical method.

As expected, for both the MAE and RMSE, the equally worst performing bands are B_8 and B_9 for all the cases considered in this study. These are higher frequency bands in which the sound power of the gun shot is relatively low (see Figure 1). At the shorter range $(r^* = 250m)$, bands of B_3 and B_7 are also relatively poor performing. Band B_7 also appears as the worst for the least uncertain MLE in the longer range $(r^* = 500m)$. All of these are the result of the model choosing the lowest value possible, the lowest value for r that was used in the computation of the likelihood, a problem that was also seen in the MLE for broadband.

The best performing band is the infrasonic band B_0, no matter which method is used or error statistic analysed. In this range the MAP method remains mostly effective. In general, the same bands (B_3, B_7, B_8, B_9) underperform as in the MLE, albeit with some small differences. Unlike for the broadband results, the MAEs for the MLE and MAP methods are equivalent when either the effective flow resistivity (σ_g) or source height (h_s) is unknown. The RMSE data suggest that the MLE is underperforming against the MAE and that outlying inferences are present in simulated data.

Comparing the broadband results (see Table 2) to the octave band results (see Table 3) suggests that overall the broadband inference is likely to outperform inference via specific octave bands for the considered acoustic and statistical models. This does not however rule out that combinations of octave band windows would allow for better inferences for some types of sources, specifically B_0, B_1 and B_2 for gunshot sources.

4.3 Octave Band Visualisations

Visualisations are completed to assess more in-depth the effects of filtering to octave bands (see Figures 10-13). Each figure is for a particular statistical method and value of the true range. Each subplot is for a given octave band where each of the plots follow the same rules as before, with each representing the given initial uncertainties. The PDF of estimates are used to assess the octave bands, so both under and over estimates can be detected.

Figure 10 depicts the PDFs for the MLE method when the true range (r^*) is 250m. Octave bands B_3, B_7, B_8 and B_9 perform poorly picking up estimates at the minimum value entered into the model. Bands B_4 and B_6 also

perform poorly but have tails extending towards to true value (r^*). The distributions created for bands B_2 and B_5 have their peaks at slightly above the minimum value, but their tails have no coverage of the true range $(r^* = 250m)$. The remaining bands, B_0 and B_1 cover much more accurately the true range (r^*) with band B_0 being the best choice for having the most likely point close to the true value. Interestingly, there is a *bimodal* (i.e. double peaked) PDF present for B_0, with an earlier peak around $120m$ which can be associated with strong variations in the gunshot spectrum (see Figure 1). B_1 has the majority of estimate below the true value but extends to the true value also. It is seen that while using the MLE method (see Figure 5) inferences can be improved by choosing the best estimates from these top-performing bands (B_0, B_1). Variation between simulations of differing input uncertainty is negligible in the case of the MLE method.

Figure 11 presents the PDFs for the error estimated using the MAP method for the true range r^*= 250m. These results follow the same behaviour as seen in the case of the MLE (see Figure 10) but with some improvements. The poor performing bands remain the same as in the case of the MLE, while the better performing bands (B_0, B_1) have larger probabilities of capturing the true range (r^*). In comparison with the MLE, the PDF for band B_1 is shifted closer to the true range. The PDF for band B_0 is accurately centred around the true value, but the *bimodality* observed in the case of MLE is now removed. The increased accuracy in the lower bands could be due to the physical interactions, i.e. excess attenuation, remaining constant at the lower frequency ranges.

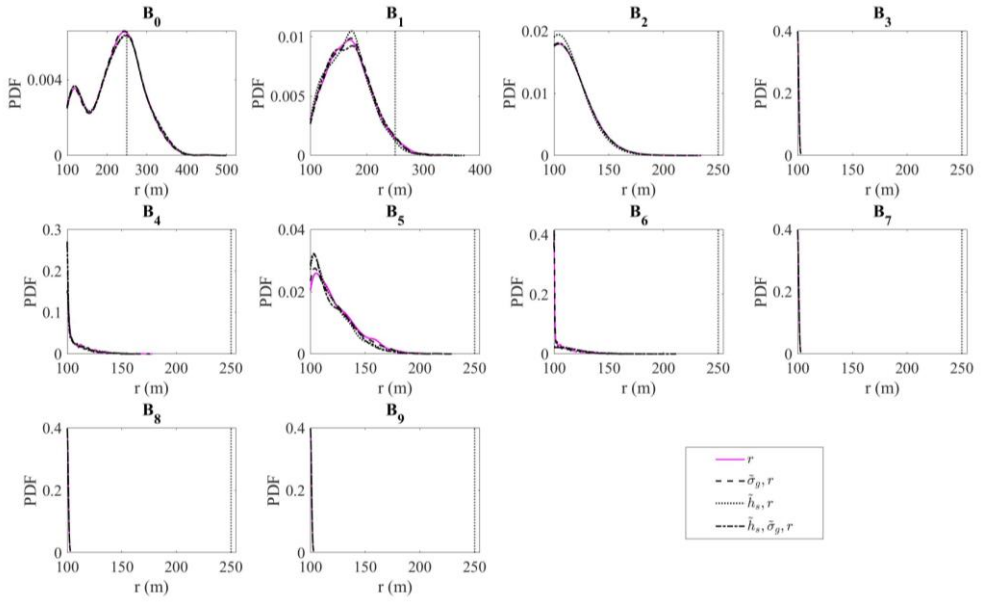

Figure 10: Kernel distributions for the PDF of estimates, using the MLE method at each octave band from smallest (top-left) to largest (bottom-right) for each simulation of varying uncertainty at $r^* = 250m$. The true range value is superimposed (dashed line) in the PDF plot of estimates.

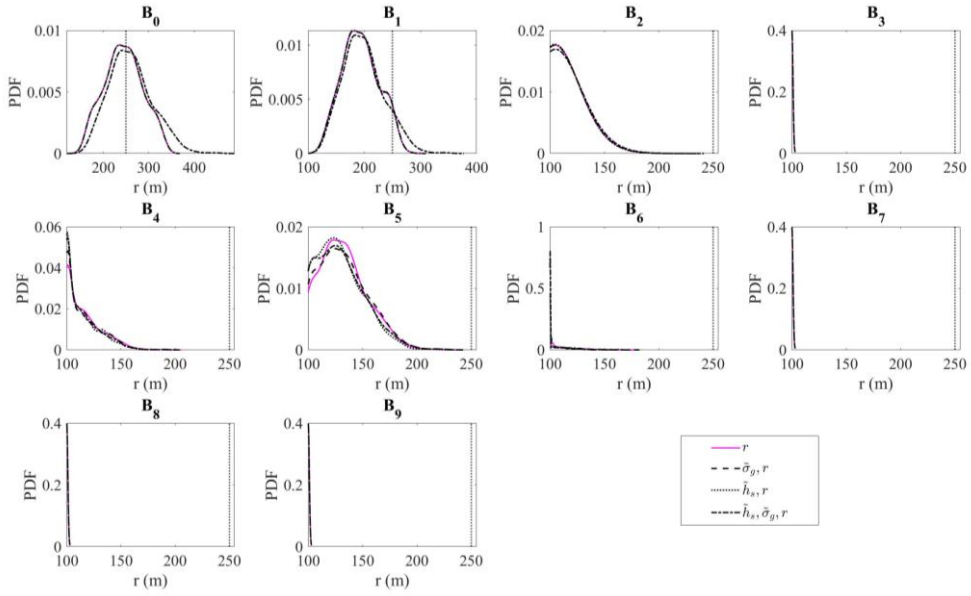

Figure 11: Kernel distributions for the PDF of estimates, using the MAP method at each octave band from smallest (top-left) to largest (bottom-right) for each simulation of varying uncertainty at $r^* = 250m$. The true range value is superimposed (dashed line) in the PDF plot of estimates.

Increasing the true range to $r^* = 500$m changes the PDFs considerably especially when using the MLE (see Figure 12). The PDFs for bands B_0, B_1 and B_2 exhibit bimodality. The two bands that can cover well the true estimate (B_0, B_1) exhibit relatively strong bimodality. In the case of band B_0 the dominant peak is around $200m$ whereas the secondary peak is close to the true range. This behaviour can hinder the convergence to the true estimate.

The application of a prior in the MAP addresses the issues experienced with the MLE method. Figure 13 illustrates that the use of limited prior knowledge removes the bimodality and leaves only one peak in the PDF for bands B_0 and B_1 close to the true estimate. The great increase in accuracy is even more likely to be due to the physical interaction patterns, which become even more constant at the extended range. The application of the MAP to other bands does not offer any improvement and results in a relatively large error.

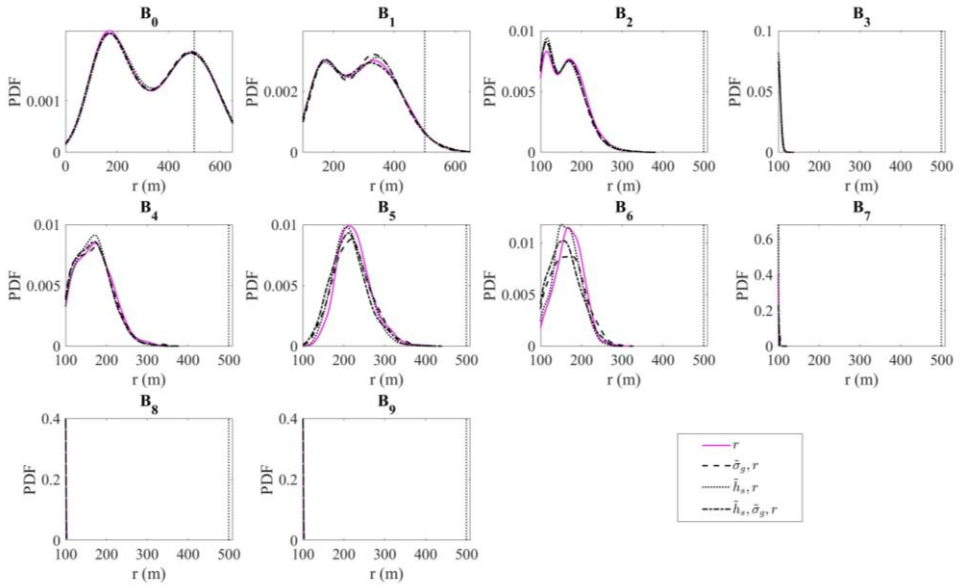

Figure 12: Kernel distributions for the PDF of estimates, using the MLE method at each octave band from smallest (top-left) to largest (bottom-right) for each simulation of varying uncertainty at $r^* = 500m$. The true range value is superimposed (dashed line) in the PDF plot of estimates.

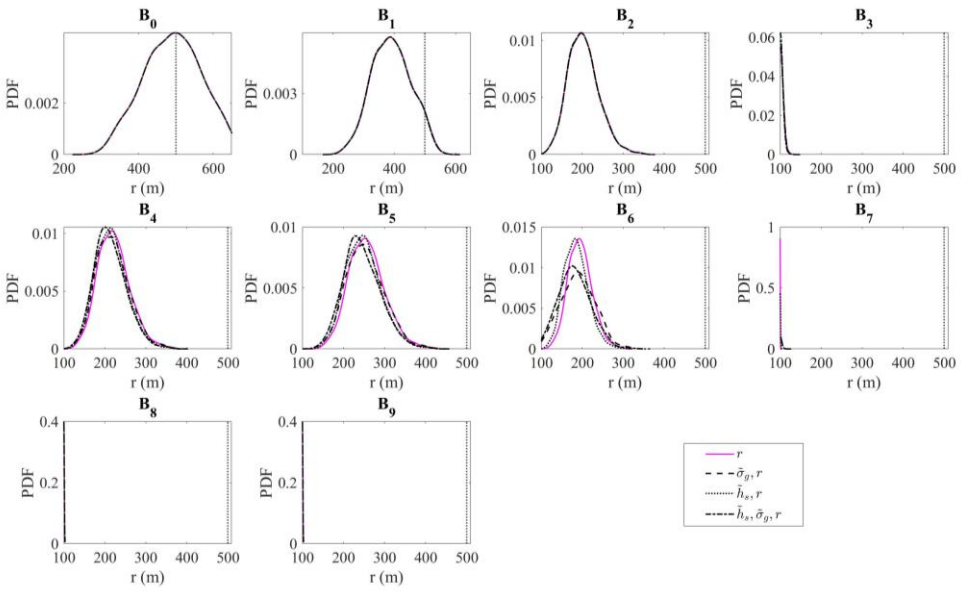

Figure 13: Kernel distributions for the PDF of estimates, using the MAP method at each octave band from smallest (top-left) to largest (bottom-right) for each simulation of varying uncertainty at $r^* = 500m$. The true range value is superimposed (dashed line) in the PDF plot of estimates.

The existence of the bimodal distribution is believed to be created by the generation of two distinct normal distributions, from the normal likelihood function (not the uncertainty – as a data doped with uniform uncertainty most times still produce normally distributed data) that are interfering with each other. Their appearance is likely due to strong interactions present at such combinations of parameters in the model.

5 Conclusions

The application of a prior to infer the true range from the sound pressure level data of a gunshot recorded on a single microphone in the presence of porous ground reduces the average error from almost 50% to within 10% of the true range event when initial information is limited to a small number of observations, e.g. $n = 10$. The MLE performs poorly because it has the tendency to choose repeatedly the smallest range possible in the model. There is a possibility for this method to become more accurate as more data for a wider range of porous grounds is made available. Application of a prior, even a flat one like in this study, greatly reduces the hindrance of parameter uncertainties. Although at the shorter range ($r^* = 250m$), the average error was only reduced to ~15% when all parameters were uncertain, indicating that shorter ranges are still more influenced by high uncertainty. Both the MLE (as long as the observation size was greatly increased) & MAP techniques are widely applicable to other acoustical settings, yet would provide a substantially effective basis to methods that incorporate *learning algorithms.*

The study of the interactions between uncertain parameters reveals that exact quantification of individual unknown parameters is not always necessary. Only at the shorter range ($r^* = 250m$) either the source height (h_s) or impedance ground (σ_g) needs quantifying to improve the inference quality as it was shown that when the both parameters (h_s, σ_g) were uncertain a notable increase in error could be observed. Further investigation into this dual uncertainty shows that the effective flow resistivity of the ground would be the preferential parameter to be quantified. This parameter seems more significant. An increasing degree of uncertainty in the adopted acoustical model becomes more influential as the range shortens.

Use of octave filtering reveals those bands which are responsible for poor or more efficient inferences. In general, limiting the analysis to a single octave band results in poor performance in terms of the MAE and RMSE in comparison with a broadband spectrum analysis. However, the PDFs of the infrasonic bands (see B_0, B_1 in Table 1) exhibit strong likelihoods on, and closely around, the given true range, especially for the MLE method, than when using the broadband spectrum. Combinations of these octave bands would likely be more effective for the inference. A large portion of energy output of a firearm exists in the infrasonic frequency range. As highlighted in recent works [6], there is strong evidence to suggest that combining octave windows between in the low and

infrasonic, frequency range will greatly improve parameter inference for firearms. Usual techniques try to use information from the supersonic projectile (bullet) which is good for 3D problems (location via miss angle), but may not actually be the best method. The lower frequency output of the firearm going off is likely to less effected by possible interferences that can generate mid and high frequency noises. This could also improve detection in more realistic environments (i.e. inhomogeneous atmosphere).

The real-life application to small arms fire is apparent. Unlike current practices [4,5], this technique does not rely on the make, model, barrel rifling etc. This makes it appropriate to such defensive security programs where quantification of the firearm would likely be implausible, but prior information of the detection zone would be readily accessible. Study into larger firearms, and other small arms fire, will help confirm the best combination of octave bands suitable for specific purposes. The main benefit of this approach is that it relies on a single receiver which can be a smartphone or low-cost microphone connected to a basic microcontroller. It should also be stated that these methods would be effective for other low frequency sources, such as the natural occurrences of earthquakes, volcanic eruptions and thunder, or man-made sources like windfarms. Further study of applications to a broader range of sources would be beneficial to test this idea further and expand it to cases where an array of receivers is used.

This study was limited to grassland. Other harder grounds can have different effects on the quality of inference methods proposed here. These proposed inference methods are not specifically exclusive to application to firearms. These can be extended to other low frequency sources such as drones and sources of environmental noise. Higher frequency sources deserve more extensive studies to assert such claims.

6 Acknowledgments

The author/s acknowledge the support of the UK's Defense Science and Technology Laboratory (Dstl) and Engineering and Physical Sciences (EPSRC) CASE studentship award to the University of Sheffield. The authors are also grateful to Prof. Jeremy Oakley from the Department of Mathematics and Statistics at the University of Sheffield for his useful comments on the statistical aspects of this work, and to fellow PhD student, Liam Grimmett (Department of Physics and Astronomy) for assistance in using the ShARC computing facilities at the University of Sheffield.

7 References

[1] D. Colton, H. W. Engl, A. K. Louis, J. McLaughlin and W. Rundell. Surveys on Solution Methods for Inverse Problems, Springer Science & Business (Dec 2012).

[2] D. K. Wilson, C. L. Pettit, V. E. Ostashev and S. N. Vecherin. "Description and quantification of uncertainty in outdoor sound propagation calculations", J. Acoust. Soc. Am., 136(3), 1013-1028. (September 2014).

[3] T. Van Renterghem, D. Botteldooren. "Variability due to short-distance favorable sound propagation and its consequences for immission assessment", J. Acoust. Soc. Am., 143(6), 3406-3417. (June 2018).

[4] K. W. Lo and B. G. Ferguson. "Localization of Small Arms Fire Using Acoustic Measurements of Muzzle Blast and/or Ballistic Shock Wave Arrivals." J. Acoust. Soc. Am., 132(5), 2997–3017. (November 2012)

[5] Lo, Kam W. "A Ballistic Model-Based Method for Ranging Small Arms Fire Using a Single Acoustic Sensor Node." J. Acoust. Soc. Am., 145(4), 2409–2417. (April 2019)

[6] J. A. Parry, K. V. Horoshenkov and D. P. Williams. "Outdoor Acoustics: Range Estimation Of Gunfire Over An Acoustically Soft Impedance Ground In A Homogeneous Atmosphere." Proceedings of the International Conference on Statistics: Theory and Applications. (Lisbon, 2019)

[7] M. S. Paolella, "Likelihood," in *Fundamental Statistical Inference: A Computational Approach*, Oxford, England: Wiley, 2018, pp. 21-27.

[8] D. Pena, C. Lima, M. Dória, L. Pena, A. Martins and V. Sousa. "Acoustic Impulsive Noise Based on Non-Gaussian Models: An Experimental Evaluation", Sensors, 19(12), 2827-2845 (Jun 2019).

[9] X. Sheng and Y.H. Hu, "Maximum likelihood multiple-source localization using acoustic energy measurements with wireless sensor networks," in IEEE Transactions on Signal Processing, 53(1), 44-53, (Jan 2005).

[10] D. Cousineau and S. Hélie, "Improving maximum likelihood estimation with prior probabilities: a tutorial on maximum a posteriori estimation and an examination of the Weibull distribution", *Tut. in Quant. Methods for Psych.,* 9(2), 61-71. (2013).

[11] D. Caviedes-Nozal and J. Brunskog, "Parameter optimization of forward sound propagation models using Bayesian inference for sound field control purposes" in Proceedings of Euronoise 2018, Crete, Greece, 2018.

[12] N. Xiang and C. J. Fackler. "Objective Bayesian Analysis in Acoustics", Acoustics Today, 11(2), 54-61. (May 2015).

[14] R. C. Maher, "Acoustical characterization of gunshots", in Proceedings of Signal Processing Applications for Public Security and Forensics Workshop 'SAFE 2007', Washington, D.C., 2007.

[15] M.E. Ylikoski, J. O. Pekkarinen, J. P. Starck, R. J. Pääkkönen and J. S. Ylikoski. "Physical Characteristics of Gunfire Impulse Noise and Its Attenuation by Hearing Protectors." International Journal of Audiology, 24(1), 3-11. (April 1994).

[16] N. E. Tsiatis, "Understanding distance shooting and the type of firearm from the analysis of gunshot sounds", Euro. Police. Sci. Res. Bulletin. 15, (Dec 2016).

[17] E.M. Salomons. Computational Atmospheric Acoustics, Kluwer Academic Publishers. (2001).
[18] O. Dazel, J.P. Groby and K.V. Horoshenkov. 'Asymptotic limits of some models for sound propagation in porous media and the assignment of the pore characteristic lengths', J. Acoust. Soc. Am., 139(5), 2463-2474. (May 2016).
[19] K. Attenborough, 'Outdoor ground impedance models', J. Acoust. Soc. Am., 129(50), 2806-2819. (May 2011).
[20] T. E. Nikolaos. (2010). "Recording and Calculating Gunshot Sound—Change of the Volume in Reference to the Distance", Proceedings of the AIP Conference, 1203(1), 846-85, (Jan 2010).
[21] Acoustics – Preferred frequencies, ISO Std. 266, 1997.
[22] J. A. Parry, K. V. Horoshenkov and D. P. Williams. "Investigating Uncertain Geometries Effect on Sound Propagation in a Homogeneous and Non-Moving Atmosphere over an Impedance Ground." Applied Acoustics, 160, 107-122 (March 2020).